POLITECNICO DI TORINO
Repository ISTITUZIONALE

Towards the definition of a benchmark for low Reynolds number propeller aeroacoustics

Original
Towards the definition of a benchmark for low Reynolds number propeller aeroacoustics / Casalino, D.; Grande, E.; Romani, G.; Ragni, D.; Avallone, F.. - In: JOURNAL OF PHYSICS. CONFERENCE SERIES. - ISSN 1742-6588. - 1909:(2021), p. 012013. (Intervento presentato al convegno 18th International Symposium on Transport Phenomena and Dynamics of Rotating Machinery (ISROMAC18)) [10.1088/1742-6596/1909/1/012013].

Availability:
This version is available at: 11583/2976910 since: 2023-03-14T09:49:50Z

Publisher:
IOP Science

Published
DOI:10.1088/1742-6596/1909/1/012013

Terms of use:
openAccess

This article is made available under terms and conditions as specified in the corresponding bibliographic description in the repository

Publisher copyright

(Article begins on next page)

12 June 2023

Journal of Physics: Conference Series

PAPER • **OPEN ACCESS**

Towards the definition of a benchmark for low Reynolds number propeller aeroacoustics

To cite this article: D. Casalino *et al* 2021 *J. Phys.: Conf. Ser.* **1909** 012013

View the article online for updates and enhancements.

You may also like

- Viscous pumping inspired by flexible propulsion
Roger M Arco, J Rodrigo Vélez-Cordero, Eric Lauga et al.

- Physics of microswimmers—single particle motion and collective behavior: a review
J Elgeti, R G Winkler and G Gompper

- Bioinspired wingtip devices: a pathway to improve aerodynamic performance during low Reynolds number flight
Michael Lynch, Boris Mandadzhiev and Aimy Wissa

This content was downloaded from IP address 130.192.232.210 on 29/03/2023 at 21:49

Towards the definition of a benchmark for low Reynolds number propeller aeroacoustics

D. Casalino, E. Grande, G. Romani, D. Ragni and F. Avallone
Aerodynamics, Wind Energy, Flight Performance and Propulsion Department, Delft University of Technology, Kluyverweg 1, 2629 HS Delft, The Netherlands

E-mail: d.casalino@tudelft.nl

Abstract. Experimental and numerical results of a propeller of 0.3 m diameter operated in quiescent standard ambient conditions at 5000 RPM and axial velocity ranging from 0 to 20 m/s and advance ratio ranging from 0 to 0.8 are presented as a preliminary step towards the definition of a benchmark configuration for low Reynolds number propeller aeroacoustics. The corresponding rotational tip Mach number is 0.231 and the Reynolds number based on the blade sectional chord and flow velocity in the whole radial and operational domain ranges from about 54000 to 106000. Force and noise measurements carried out in a low-speed semi-anechoic wind-tunnel are compared with scale-resolved CFD and low-fidelity numerical results. Results identify the experimental and numerical challenges of the benchmark and the relevance of fundamental research questions related to transition and other low Reynolds number effects.

1. Introduction

The development of tools for the design and optimization of propellers employed in multi-copter unmanned air vehicles and drones has to face two major difficulties. The first one is the availability of reliable force, flow and noise data acquired for the same experiment in controlled conditions. The second difficulty is related to the intrinsic limits of scale-resolved CFD methods to capture low Reynolds number phenomena like transition and the occurrence of laminar separation bubbles.

Recent attempts to validate Lattice-Boltzmann Method / Very Large Eddy Simulation (LBM/VLES) results [1] revealed that the flow recirculation induced by a rotor operated in a confined environment, and the consequent interaction between blades and turbulent eddies, generates high-order Blade-Passing Frequency (BPF) loading noise harmonics. Similar observations have been made in other experiments [2]. Other sources of experimental uncertainties are: (i) the vibration of the test rig resulting in additional sources related to the random blade motion [3], (ii) the presence of electric motor noise, which is affected by the rotor torque [4] and thus not easily separable from the rotor aerodynamic noise, or treatable as a background noise contribution, and (iii) the flow regime at several radial stations (laminar/turbulent, attached/separated) and the presence of laminar separation bubbles. In the case of non-axial flow conditions, additional complications arise due to the periodic inflow variation and the necessity to characterize flow hysteresis mechanisms, while mitigating the higher vibrations of the rig. On the numerical side, the main challenges are related to the capability of the CFD solver to predict the correct transitional flow behavior. Scale-resolved methods like LBM/VLES [5] or Detached Eddy Simulation [6] (DES), or different variants of hybrid Reynolds Averaged Navier-Stokes

Content from this work may be used under the terms of the Creative Commons Attribution 3.0 licence. Any further distribution of this work must maintain attribution to the author(s) and the title of the work, journal citation and DOI.
Published under licence by IOP Publishing Ltd

(RANS) / Large Eddy Simulation (LES) methods are typically used for aeroacoustic purposes as a faster alternative to LES. However, hybrid methods have to deal with the "grey-area" related problem of finding the balance between eddy viscosity in the scale-modelled flow region and the need of not anticipating separation on smooth surfaces and not preventing transition in boundary layers and wakes [7, 8]. Broadband noise is generated by the interaction between boundary layer turbulence and the trailing edge, by the impingement of inflow turbulence on the leading edge, and by Blade-Vortex Interaction (BVI) at very low or negative advance ratios. Trailing edge noise prediction, in particular, relies on the capability to predict transition with low-intrusive tripping devices like zig-zag strips [9, 10] or synthetic turbulence generators [11].

Capturing the correct boundary layer properties of low Reynolds number propellers is also crucial for the sake of accurate thrust and torque predictions. Typical turbulence closure models used in RANS solvers suffer to predict the correct near-wall behavior of turbulent flows and do not provide reliable predictive capabilities of transitional flows [12]. Low-fidelity methods based on the Blade Element Momentum Theory (BEMT) and two-dimensional airfoil lift and drag coefficients computed via coupled panel/boundary-layer models like Xfoil [13] can provide satisfactory accuracy, beyond the common expectation, at sufficiently high advance ratios [14]. Unfortunately, BEMT methods suffer for the inaccurate 2D prediction of stall and post-stall behavior of highly loaded blade sections close to the hub at low advance ratios [15, 16] and for the inaccurate modelling of the near-wake induction effects, again, at low advance ratios [14].

The goal of the present paper is to address the aforementioned experimental, numerical and modelling challenges by comparing preliminary experimental, scale-resolved LBM/VLES and low-fidelity BEMT results, and thus progress towards the definition of a benchmark problem for low Reynolds number propeller aeroacoustics. This is part of a research initiative aimed at investigating the different broadband noise generation mechanisms and the properties of transitional flows at different radial stations and for different operating conditions.

The paper is organized as follows. The physical and digital test environments and the propeller geometry are described in section 2. Information about the measurement techniques and a short description of the LBM/VLES and the BEMT-based propeller noise model are provided in section 3. Experimental, low- and high-fidelity numerical results are reported and discussed in section 4. The main conclusions of the present work are finally drawn in the conclusive section.

2. Test rig and physical/digital environment

The test rig installed in the semi-anechoic aeroacoustic wind tunnel of Delft University of Technology (TU-Delft A-Tunnel) is shown in figure 1. The flow is coming from the circular nozzle installed on the floor of the test chamber. The nozzle diameter is 0.6 m, the height of the test chamber is 3.2 m, and the other two dimensions are 6.4 m and 4.4 m. The cut-off frequency of the chamber is approximately 200 Hz. The turbulence levels in the core of jet are below 0.05% and flow non-uniformity in the nozzle area is below 0.5% for the a nozzle exit velocity of 35 m/s.

The propeller is connected to a profiled aluminum cylindrical nacelle for minimum interference with the propeller flow, within which the motor, an encoder, a load cell and a torque cell are embedded. The nacelle is supported by stiffened hollow aluminium NACA 0012 profiles of 6 cm chord, inside which the cabling is housed and remotely connected to the instrumentation. The entire structure is held up above the nozzle of the tunnel by four steel wire tubes of 2 cm diameter fixed to the tunnel. The entire rig is very stiff and submitted to almost no vibration when the rotor is operated in axial flow conditions, as in the present preliminary campaign. The nacelle hosts the propeller drivetrain, which consists of: (i) an electrical brushless motor Leopard Hobby LC2830 of 27.8 mm diameter and 216 W maximum power; (ii) a Broadcom incremental optical encoder to measure the shaft rotational speed, which consists of a rotating disk, a light source and a photo detector; (iii) a load cell Futek LSB200 with a capacity of 22.2

N for the thrust measurement; (iv) a Transducer Techniques RTS 25 with a capacity of 0.18 Nm for torque measurements. The distance between the rotor plane and the jet exhaust plane is about 0.5 m. An exploded view of the propeller drivetrain is shown in figure 2.

Figure 1. Test rig in TU-Delft A-Tunnel.

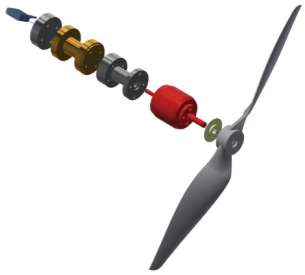

Figure 2. Exploded view of the propeller drivetrain.

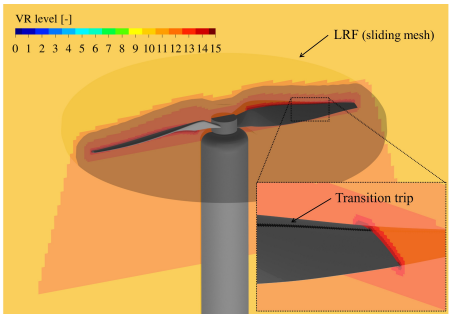

Figure 3. PowerFLOW computational setup and mesh layout.

Full anechoic environment conditions are conditions are modelled in the digital PowerFLOW setup, by considering a very large simulation domain with outer acoustic sponge layers. The inner part of the simulation domain is shown in figure 3, where mesh regions of Variable Resolution (VR) are identified by different colors. The finest resolution level (VR15) is defined through an offset of the blade zig-zag trip and trailing-edge, while the second finest one (VR14) is defined as an offset of the blade surface. In order to force the VLES model to switch from modelled to resolved turbulence, a zig-zag trip of 0.17 mm height is located at 25% of the chord on the blade suction side.

In section (4), results are reported for a mesh resolution corresponding to 2600 voxels/D (with $D = 0.30$ m being the propeller diameter) in the blade offset region (VR14). The grid independence of both forces and far-field noise has been verified.

The propeller employed for this experiment is derived from a two-bladed APC-96 model, by reshaping each single profile with a NACA4412 and rescaling the size to 15 cm tip radius. An elliptical root section is merged with the profiled section starting from a radius of 1 cm ($r/R = 0.06$). The hub radius is 1.25 cm. An image of the propeller is shown in figure 4. The chord and twist radial distribution are plotted in figure 5. The propeller, made of steel alloys, was manufactured using CNC machine and successively laser scanned to measure deviations from the CAD model of the twist distribution and other constructive parameter. The interest of using this model instead of the original off-the-shelf one resides in: (i) the possibility to deliver a CAD model and the analytical description of the constructive parameters as part of the benchmark definition, (ii) the possibility to control manufacturing tolerances, (iii) and the high stiffness of the model, thus guaranteeing negligible elastic deformations in operation.

The propeller is operated by varying the jet wind tunnel velocity and the motor RPM to obtain a range of advance ratio $J = V_0/(nD)$ from 0 to 0.8, V_0 denoting the free-stream axial flow velocity and n the number of rotor revolutions per second. In the present paper, only results for the jet exit velocities of 0, 10 and 20 m/s and 5000 RPM are considered, corresponding to $J = 0$, 0.4, and 0.8, respectively.

3. Tools and methods

In this section, an overview of the employed experimental and numerical techniques is provided.

3.1. Noise measurements

Noise measurements are performed through microphones mounted on a circular arc, but only results for one microphone at the position $(0.444, 0.0, 1.402)$ m (reference system in figure 4) are

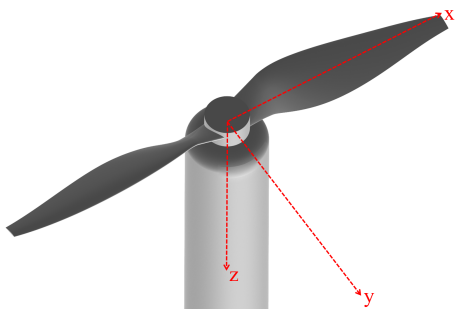

Figure 4. Propeller geometry and reference system.

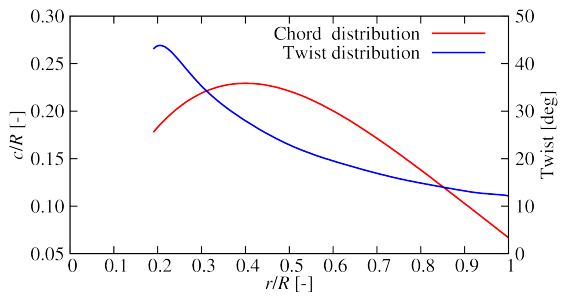

Figure 5. Propeller chord and twist distributions.

reported for the sake of compactness. The microphone array consists of 8 LinearX M51 pre-amplified microphones (frequency response: ±1 dB in the frequency range of 10 Hz to 40 kHz, maximum output: 150 dB). A sampling frequency of 50 kHz and a recording time of 60 s are used for each measurement by using a NI-9234 4-channel, dynamic signal acquisition module. The acoustic data are separated in time blocks of 8192 samples for each Fourier transform and windowed using a Hanning weighting function with 50% window overlap, thus providing a frequency resolution of about 5 Hz.

3.2. BEMT-based model

A conventional BEMT formulation with uniform inflow and Prandtl tip-losses correction is employed. The required blade sectional forces are computed using the boundary layer model by Drela [13] implemented in the BEMT tool. Aerodynamic polars are pre-computed with an angular step of 1 deg in the angle of attack range from $-15°$ to $15°$, and at five values of the Reynolds number covering the whole range of radial variation. For the sake of numerical robustness and efficiency, all quantities employed by the iterative BEMT algorithm (sectional aerodynamic coefficient and stall angles) and by the broadband noise model (boundary layer properties at the trailing edge) are polynomially fitted with respect to the radial coordinate and the angle of attack. Post-stall lift and drag coefficients are computed using Viterna & Corrigan approach [17]. The radial distribution of the blade sectional force and the sectional airfoil surface are used to define the input of a time-domain FW-H noise computation based on the compact dipole and monopole formulation by Casalino et al. [18]. This provides the tonal noise contribution, whereas broadband noise is computed using the trailing edge noise model by Roger & Moreau's [19], extended to a rotating blade [20] and by using Schlinker & Amiet's empirical wall pressure model [21], which is based only on boundary layer edge velocity and displacement thickness at 95% of the chord, computed by the airfoil boundary layer model. A similar broadband noise prediction procedure has been used by other authors in the past [22, 23].

3.3. LBM/VLES flow solver

The SIMULIA PowerFLOW solver, version 6-2019, has been used in the present work. The properties of this software and its suitability for aeroacoustic applications are widely discussed in the literature, covering both aerospace, automotive and wind-energy applications. Referring to noise from rotating parts, the following benchmark works can be quoted: small UAV rotors [1], car cooling fans [24], aircraft propellers [25], aero-engine fan/OGV stages [9, 26], and helicopter rotors [27]. PowerFLOW is based on a Cartesian mesh LBM with automatic mesh generation, with no restriction on the geometric complexity of the models that can be treated. Fully automatic workflows, from case preparation to results post-processing, can be easily developed,

as for complex thrust-vectoring multi-copter eVTOL vehicles [5], for which an entire flight envelop can be explored in reasonable times by running multiple jobs on a HPC cloud system.

LBM is intrinsically unsteady and compressible. It is based on the idea of statistically tracking the advection and collisions of fluid particles by an integer number of distribution functions aligned with predefined discrete directions. Flow variables such as density and velocity are computed by taking the appropriate moments, i.e., summations over the set of discrete directions of the particle distribution function [28]. The relaxation time and other parameters of the equilibrium distribution function are computed by considering scales related to the turbulent motion of the resolved flow field, computed using a two-equation transport model based on the $k-\epsilon$ re-normalization group theory [29, 30]. Conversely to RANS models, Reynolds stresses are not explicitly added to the flow governing equations, but are a consequence of an alternation of the gas relaxation properties that lead the flow towards a state of dynamic equilibrium. This is the essence of the LBM/VLES model: an extension of the kinetic theory from a gas of particles to a gas of eddies, which can be also interpreted as the application of a Boussinesq model at lattice Boltzmann level. It can be demonstrated that the effective Reynolds stresses have a non-linear structure and are better suited to represent turbulence in a state far from equilibrium, such as in the presence of distortion, shear and rotation [31].

4. Results and discussion

Figure 6 shows iso-surfaces of λ_2 (value $-1.5 \cdot 10^6$), colored by vorticity magnitude in the range from 0 to 10^4 1/s, for the case $J = 0.4$. A well developed turbulent boundary layer trigged by the zig-zag strip can be observed on the blade suction side. In the absence of experimental evidence of the real boundary layer status, forcing an explicit transition on the suction side and not on the pressure side constitutes the largest source of numerical uncertainties in the present study. Indeed, the preliminary tests were performed using untripped blades, while, in future tests, the effects due to tripping will be systematically investigated. Moreover, the boundary layer transitional status along the blade for untripped cases will be characterized by using optical diagnostic techniques.

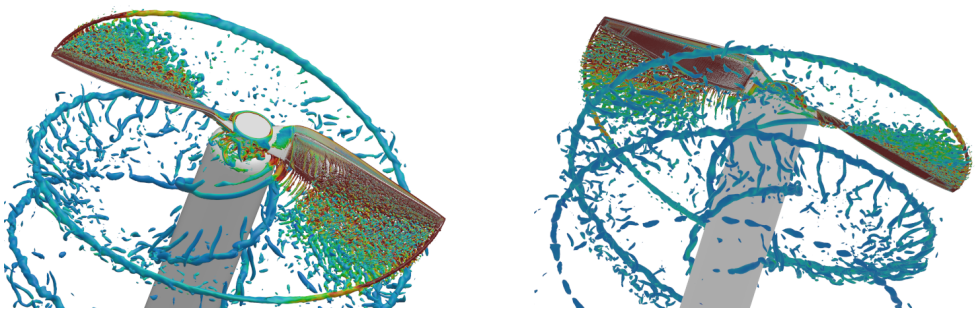

Figure 6. Iso-surfaces of λ_2 at $J = 0.4$ on the blade suction (left) and pressure side (right).

Contour plots of the time-average velocity magnitude in a meridian plane are shown in figure 7 for the three values of J. Interestingly, for the highest value of J the slipstream velocity is very close to the free-stream value, which corresponds to a condition of zero thrust. Instantaneous vorticity magnitude on the same plane is shown in figure 8. The typical tip-vortex pattern with trailing and blade junction vortices is visible. For the hover condition (zero advance ratio), the rotor wake is less organized and the occurrence of BVI can be observed.

Results of thrust and torque coefficients are shown in figure 9 and 10. As mentioned, the grid independence of the LBM/VLES solution has been verified. Compared to experiments, thrust is predicted in a satisfactory way along the whole range of advance ratio, and the agreement

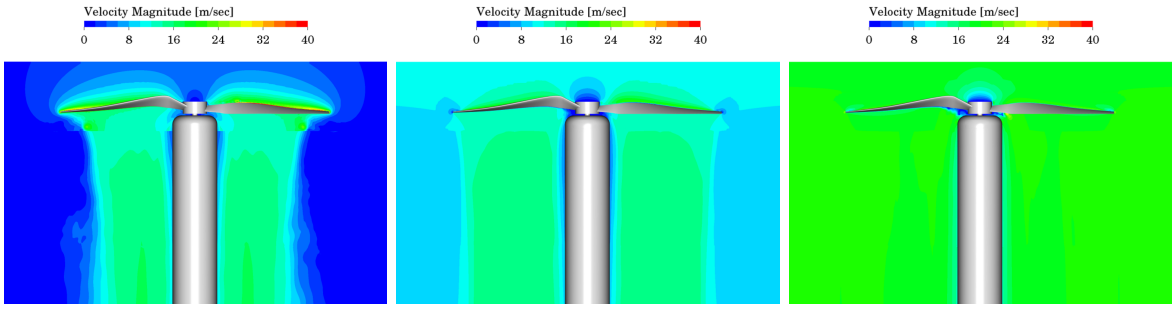

Figure 7. Time-average velocity magnitude for $J = 0$ (left), 0.4 (middle) and 0.8 (right).

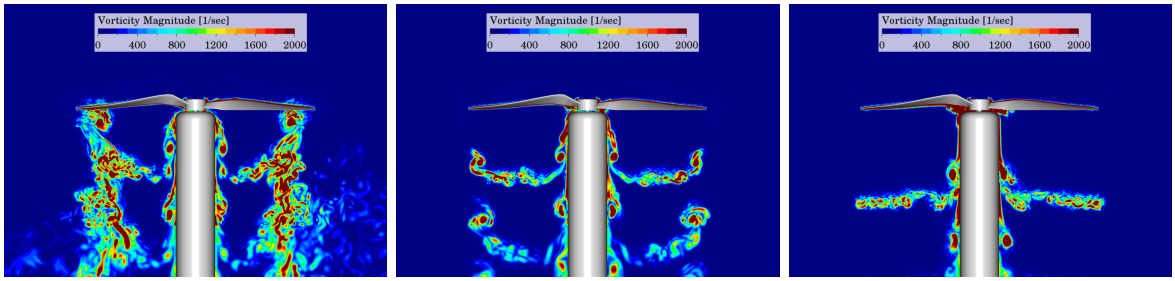

Figure 8. Instantaneous vorticity magnitude for $J = 0$ (left), 0.4 (middle) and 0.8 (right).

between low- and high-fidelity results is excellent. The zero-thrust condition around $J = 0.8$ is also well predicted by both LBM/VLES and BEMT. Torque is fairly well predicted by the LBM/VLES, with a higher discrepancy with respect to the measurements in hover, whereas a significant underestimation can be observed for the BEMT solution. Further investigation are needed to understand the cause of this inaccuracy, but very likely this is due to delayed prediction of the turbulence transition on the suction side of the blades.

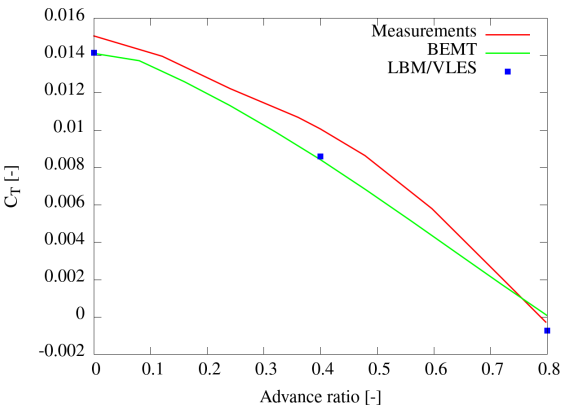

Figure 9. Thrust coefficient.

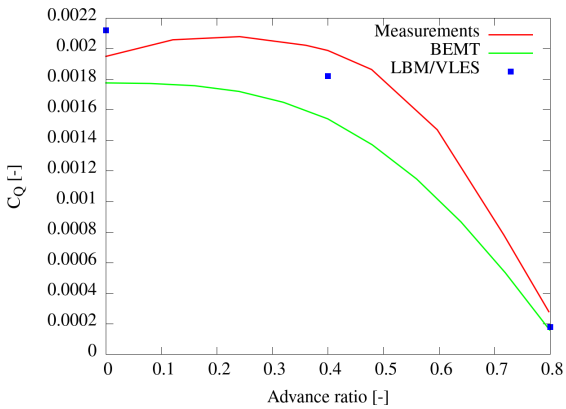

Figure 10. Torque coefficient.

Finally, noise spectra at the reference microphones are shown in figures 11. As already pointed out, the test chamber has a cut-off frequency around 200 Hz, the BPF value being 167 Hz. As a consequence, measured noise spectra below this frequency are affected by the chamber reverberation and are not fully reliable for quantitative comparisons. Another limitation of the

present experimental dataset is related to the wind-tunnel background noise, which overwhelms the propeller noise at the highest reported advance ratio. It should be also pointed out that the measured noise spectra exhibit a tone at the shaft frequency (0.5 BPF), which is due to an imperfect balancing of the rotor. In hover conditions, high-order BPF tones were measured, which are due to additional unsteadiness and consequent rig vibration caused by a weak Blade-Vortex Interaction (BVI) occurring at zero advance ratio. At frequencies above about 5 kHz, the measured spectra are affected by a modulation pattern probably due to a reflection taking place on the metallic support of the microphone, and exhibit sharp tones generated by the electric driver. All these artefacts of the experimental rig and associated uncertainties will be characterized in future publications.

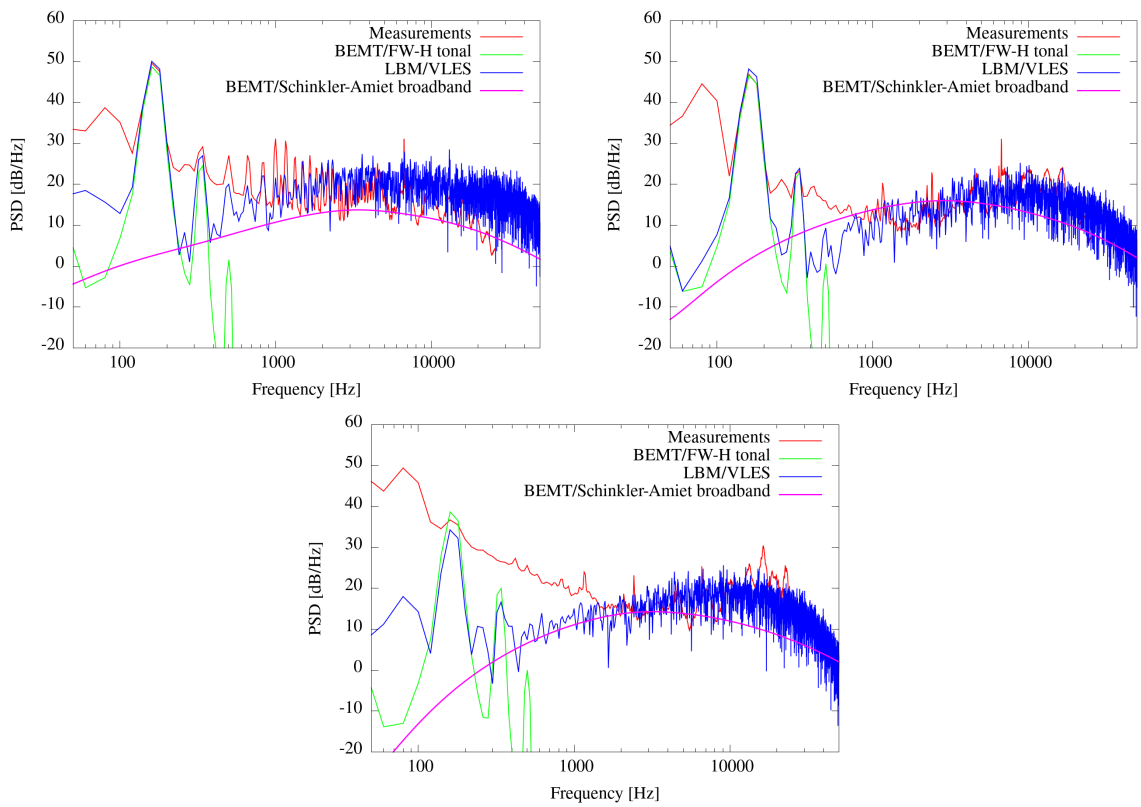

Figure 11. Noise power spectral density at different advance ratios: J=0 (top left), J=0.4 (top right) and J=0.8 (bottom). Comparison between measurements, BEMT tonal results, semi-analytical broadband results based on Schlinker & Amiet's wall pressure model and PowerFLOW/FW-H results.

Consistently with the force prediction, the BEMT-based approach is able to predict reliable BPF tonal levels that compare very well with the LBM/VLES prediction for the three advance ratios. Analytical trailing edge noise predictions based on Schlinker & Amiet's wall pressure model are also plotted. These results have been obtained with a convection velocity coefficient of 0.65 and a spanwise correlation coefficient of $b_c = 1.5$ in Roger & Moreau's formulation, without any further tuning. The predicted trends are in fairly good agreement with the PowerFLOW prediction at all the advance ratios considered, confirming that the main broadband noise generation mechanisms taking place in the scale-resolved flow simulation is indeed turbulent boundary layer trailing edge noise, thus justifying the use of trip in the PowerFLOW simulations. The PowerFLOW results are in quite good agreement with the measurements up to a frequency

of about 7 kHz, above which the present measurements are contaminated by a combination of electric motor noise and sound reflections. In hover condition, the analytical broadband noise prediction provides lower levels than the LBM/VLES prediction, which could be explained by the occurrence of a weak BVI.

5. Final remarks and outlook

A preliminary step towards the definition of a benchmark problem for small UAV propeller aeroacoustics was accomplished through comparisons between measurements and low-/high-fidelity predictions. LBM/VLES simulations were performed by triggering the boundary layer transition on the suction side, without a clear knowledge of the real flow regime in the untripped physical tests. However, the favourable agreements between measured and predicted broadband noise levels supported the presence of a transitional flow regime, at least in the outer part of the blade suction side. The analytical trailing edge noise model underestimates the broadband noise levels in hover conditions, which confirms the hypothesis of BVI induced noise, as from the observation of LBM/VLES flow solutions.

During the reported tests, phase-locked stereo PIV measurements have been carried out, which will be exploited to shed light on the boundary layer regime. Moreover, the experimental campaign will be repeated in order to address the effects of boundary layer tripping and improve the quality of the far-field noise measurements.

References

[1] Nardari C, Casalino D, Polidoro F, Coralic V, Brodie J and Lew P T 2019 *AIAA Paper 2019-2497*
[2] Stephenson J H, Weitsman D and Zawodny N S 2019 *Journal of Acoustic Society of America* **145** 1153
[3] McKay R and Kingan M J 2019 *AIAA Paper 2019-2499*
[4] Henderson B S and Huff D 2018 *AIAA Paper 2018-2953*
[5] Casalino D, van der Velden W and Romani G 2019 *AIAA Paper 2019-1834*
[6] Ventura Diaz P and Yoon S 2018 *AIAA Paper 2018-1266*
[7] Batten P, Goldberg U and Chakravarthy S 2004 *AIAA Journal* **42** 485–492
[8] Mockett C, Haase W and Schwamborn D 2018 *Go4Hybrid: Grey Area Mitigation for Hybrid RANS-LES Methods* (Springer)
[9] Casalino D, Hazir A and Mann A 2018 *AIAA Journal* **56**
[10] Casalino D, Avallone F, Gonzalez-Martino I and Ragni D 2019 *Journal of Sound and Vibration* **442** 138–154
[11] Shur M L, Spalart P R, Strelets M K and Travin A K 2014 *Flow, Turbulence and Combustion* **93** 63–92
[12] Di Pasquale D, Rona A and Garrett S J 2019 *AIAA Paper 2019-3812*
[13] Drela M 1989 *XFOIL: An Analysis and Design System for Low Reynolds Number Airfoils. In: Mueller T.J. (eds) Low Reynolds Number Aerodynamics. Lecture Notes in Engineering, vol 54* (Springer, Berlin, Heidelberg)
[14] Gur O and Rosen A 2008 *The Aeronautical Journal* **112** 689–704
[15] Uhlig D V and Selig M S 2008 *AIAA Paper 2008-407*
[16] McCrink M H and Gregory J W 2015 *AIAA Paper 2015-3296*
[17] Viterna L A and Corrigan R D 1981 *NASA N83 19233*
[18] Casalino D, Barbarino M and Visingardi A 2011 *AIAA Journal* **48** 1614–1624
[19] Roger M and Moreau S 2005 *Journal of Sound and Vibration* **286** 477–506
[20] Amiet R K 1974 *NASA N212775-1*
[21] Schlinker R H and Amiet R K 1981 *NASA CR-3470*
[22] Rozenberg Y, Roger M and Moreau S 2010 *AIAA Journal* **48** 951–962
[23] Pagano A, Barbarino M, Casalino D and Federico L 2010 *AIAA Journal of Aircraft* **47** 835–848
[24] Piellard M, Coutty B B, Le Goff V, Vidal V and Perot F 2014 *AIAA Paper 2014-2455*
[25] Avallone F, Casalino D and Ragni D 2018 *International Journal of Aeroacoustics* **17**
[26] Gonzalez-Martino I and Casalino D 2018 *AIAA Paper 2018-3919*
[27] Romani G and Casalino D 2019 *Aerospace Science and Technology* **800** 147–157
[28] Shan X, Yuan X F and Chen H 2006 *Journal of Fluid Mechanics* **550** 413–441
[29] Yakhot V and Orszag S A 1986 *Journal of Scientific Computing* **1** 3–51
[30] Pervaiz M and Teixeira C M 1999 *ASME PVP Am Soc Mech Eng Press Vessels Pip Div* **397**
[31] Chen H, Orszag S, Staroselsky I and Succi S 2004 *Journal of Fluid Mechanics* **519** 301–314